O. S. Galaktionov, P. D. Anderson, G. W. M. Peters, H. E. H. Meijer*

Materials Technology, Eindhoven University of Technology, Eindhoven, The Netherlands

Analysis and Optimization of Kenics Static Mixers

The mapping approach is applied to study the distributive mixing in the, widely industrially used, Kenics static mixer. The flexibility of the mapping method makes it possible to study and compare thousands of different mixer layouts and perform optimization with respect to macroscopic homogenization efficiency and interface generation. In the paper two different designs of the mixer are investigated. The conventional mixer with sequentially different twisted blades and adesign where the twist direction is maintained constant. In both cases the blade twist angle is varied. Recommendations are given in the choice of the design of the mixer dependent on the desired structure of mixing.

1 Kenics Static Mixer: Introduction

1.1 Mixer Geometry

The underlying idea of the Kenics mixer (and all other staticmixers) is to mimic the "Baker's transformation" [1, 2] by repeatedly cutting, re-orienting and stacking material to produce a multitude of striations. The Kenics static mixer is a typical in-line mixing device. It consists of a cylindrical pipe with mixing elements fixed inside. The mixing elements are formed by helically twisted rigid plates (usually of the same pitch), each dividing the pipe into two twisted semicircular ducts. The inserts are placed tightly one after another so that the leading edge of the next insert is perpendicular to the trailing edge of the previous one. The flow along the pipe is driven by a pressure gradient. Although such mixers are also used at moderate ($\sim 10^2$) Reynolds numbers, we consider the most common case of Stokes flow of viscous fluids, where the inertial forces can be neglected. The mixer configuration as used by *Avalosse* and *Crochet* [3] is taken as a starting point. The inner diameter of the pipe is 60 mm, the length of the 180°-twisted blade equals 115 mm, while its thickness (2 mm) is neglected here for simplicity. (This assumption seems not to cause any noticeable differences in the mixer's operation, see the results of [3].) Layouts with blades of different twist direction (both left- and right-oriented) will be considered, and we change the total blade twist angle while keeping the pitch of the blades the same as in *Avalosse* and *Crochet* [3]. Thus, changing the total blade twist means actually changing the blade length.

Fig. 1 shows three typical examples of mixer configurations. Although the methods used in the current work easily allow for higher flexibility, we will mostly limit the analysis to mixers that are spatially periodic with a repeating period sequence of exactly two blades of the same absolute twist (except in subsection 4.1), but possibly with a different twist direction. The obvious reason is that because of the working principle of the Kenics mixer, not much improvement can be expected from symmetry-breaking measures (that are rather successful in prototype mixing flows [4 to 7]), e. g. by combining long and short blades. Under these limitations two basic types of design exist [8]: a layout with alternating right and left twist direction, referred to as "RL", and the layout with blades in the same direction of the twist, referred as "RR". Since it was shown in [9] that the pitch angle has a rather minor effect on mixer performance, it is fixed in the current work, and the only parameter to change is the total blade twist angle. Throughout this chapter we will use the "RR" or "RL" notation for the type of geometry together with the blade twist angle (in degrees) to specify a particular mixer geometry. Thus, for example RL-180 stands for the mixer, combining the blades twisted 180° in both directions, Fig. 1A, as analyzed in [3]. Fig. 1B shows the RR-180 configuration as was considered by *Hobbs* and *Muzzio* [8], while Fig. 1C illustrates the RL-120 geometry, which was suggested as more energy efficient in [9].

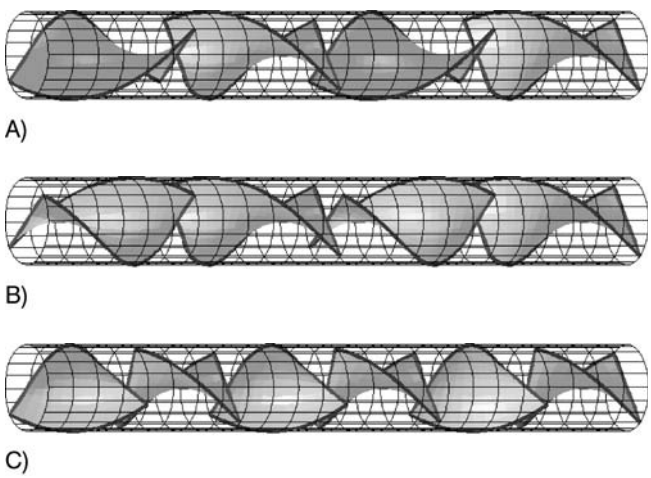

Fig. 1. Examples of different Kenics designs, A: a "standard" right-left layout with 180° twist of the blades (RL-180); B: right-right layout with blades of the same direction of twist (RR-180); C: (RL-120) right-left layout with 120° blade twist

* Mail address: P. D. Anderson, Materials Technology, Eindhoven University of Technology, 5600 MB Eindhoven, The Netherlands

1.2 Principle of Kenics Operation

The Kenics mixer in general is intended to mimic to a possible extent the "bakers transformation" (see [1]): repetitive stretching, cutting and stacking. To illustrate the principles of the Kenics static mixer a series of the concentration profiles inside the first elements of the "standard" (RL-180) are presented in Fig. 2. All these concentration distributions are obtained using the mapping approach. The first image shows the initial pattern at the beginning of the first element: each channel is filled partly by black ($c = 1$) and partly by white ($c = 0$) fluid, with the interface perpendicular to the blade. The flux of both components is equal.

The images in Fig. 2B to E show the evolution of the concentration distribution along the first blade, the thin dashed line in Fig. 2E denotes the leading edge of the next blade. From the point of view of mimicking the bakers transformation it seems that the RL-180 mixer has a too large blade twist: the created layers do not have (even roughly) equal thickness. The configuration achieved $1/4$ blade twist earlier (Fig. 2D) seems to be much more preferable. The next frame, Fig. 2F, shows the mixture patterns just 10° into the second, oppositely twisted, blade. The striations, created by the preceding blade are cut and dislocated at the blade. As a result, at the end of the second blade (Fig. 2G) the number of striations is doubled. After four mixing elements, Fig. 2H, sixteen striations are found in each channel. The Kenics mixer roughly doubles the number of striations with each blade, although some striations may not stretch across the whole channel width. Note, that the images in Fig. 2 show the actual spatial orientation of the striations and mixer blades. In all further figures the patterns are transformed to the same orientation: the (trailing edge of the) blade is positioned horizontally. This simplifies the comparison of self-similar distributions.

1.3 Existing Approaches to Kenics Mixer Characterization

The widespread use of the Kenics mixer prompted the attention to the kinematics of its operation and attempts to find ways to improve its performance. *Khakhar* et al. [10] considered the so-called *partitioned pipe mixer*, designed to mimic the operation of Kenics. The analogy is incomplete, since the partitioned pipe mixer is actually a dynamic device, consisting of rotating pipe around a number of straight, fixed, perpendicular placed, rectangular plates[1]. This device, however, gives the possibility to control its efficiency by changing the rotation speed of the pipe (which may be considered to be analogous to the twist of the blades in a Kenics mixer) and allowed relatively simple mathematical modeling using an approximate analytical expression for the velocity field. The expression for the velocity field (and, consequently, the numerical simulations) was improved by *Meleshko* et al. [11], achieving even better agreement with experimental results of [10]. However, these studies were dealing with a simplified model, which fails to catch the details of the real flow in a Kenics static mixer.

The increasing computational power allowed different researchers to perform direct simulations of the three-dimensional flow in Kenics mixers [3, 8, 12 to 16]. The last paper considers even flows with higher Reynolds numbers up to $Re = 100$. These studies analyzed only certain particular flows and, unlike [10], did not allow for the optimization of the mixer geometry, due to high cost of 3D simulations.

More systematic efforts on exploring the efficiency of the Kenics mixer were made by [9], who suggested a more energy efficient design with a total blade twist of 120°. They explored different mixer configurations, but, since the velocity field had to be re-computed every time, the scope was limited: only seven values of the blade twist angle were analyzed. The aim of the current work is to study numerically the dependence of the mixer performance on the geometrical parameter (blade twist angle) and to determine the optimal configuration within the imposed limitations. Since it was shown in [9] that the blade pitch has rather minor effect on mixer performance, it is fixed in the current work.

The Kenics static mixer was also considered as a tool to enhance the heat exchange through the pipe walls [17]. They found that the Kenics mixer may offer a moderate improvement in heat transfer, but its applicability in this function is limited by difficulty of i. e. wall cleaning. However, only mixers with the "standard" 180° blade twist were considered. In the current work we also analyse the influence of the blade twist angle on refreshing of material on the tube surface. Recently *Fourcade* et al. [16] addressed the efficiency of striation thinning by the Kenics mixer both numerically and experimentally, using the so-called "striation thinning parameter" that describes the exponential thinning rate of material striations. This

[1] Note that the partioned pipe mixer is actually a simplified model of a RR type of Kenics mixer

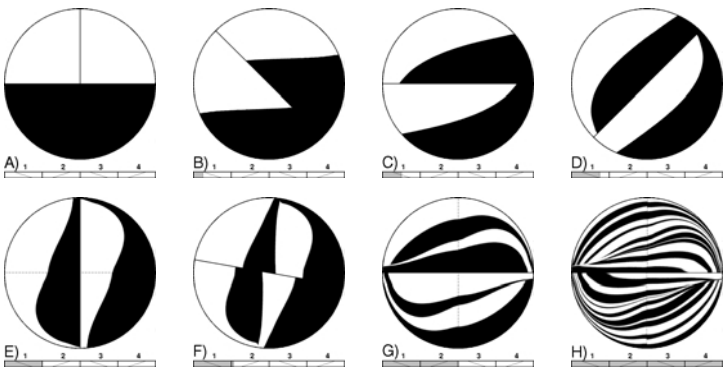

Fig. 2. How the Kenics mixer works: the frames show the evolution of concentration patterns within the first four blades of the RL-180 mixer

was done by inserting a large number of "feed circles" and numerically tracking markers along the mixer. Their method allows to characterize the efficiency of the static mixer. However, adjusting the geometry would necessitate repetition of all particle tracking computations. Optimization of the mixer geometry calls for a special tool that allows to re-use the results of tedious, extensive computations in order to compare different mixer layouts. A good candidate for such a tool is the mapping technique.

In this work we take into account the most important results of [9]. The mapping method is used to systematically study the performance of Kenics mixers of different geometries (twist direction and angle of the blades) and to find its optimal design.

2 Application of the Mapping Technique to the Kenics Mixer

2.1 Computational Domain

To implement the mapping approach, the Kenics static mixer is subdivided into independent functional mixing modules. These modules are assembled in an appropriate sequence to obtain the real mixer design. An essential requirement is that the flow inside a module can be assumed to be independent on the preceding or following ones. The starting point is to select a computational domain that contains all necessary features of the mixer, see Fig. 3A. The direction of the fluid flow is upwards and although the configuration is simple, it fulfills our requirements:

- In order to obtain a fully developed flow in the entrance and exit conditions *inflow and outflow sections* are provided with flat blades that subdivide the tube into two straight semicircular ducts for which an analytical expression, known ina closed form [11], is used to specify the boundary conditions.
- In its *central section* the flow domain considered contains a long right-twisted blade with total twist angle of 180°. It is assumed (and has yet to be verified) that in the middle zone of the blade, the velocity field is independent of the axial coordinate, if viewed in a properly rotated reference frame, aligned with the blade.
- The flat blade in the *lower section* changes into a right-twisted blade (with total twist of 90°) that forms a R-R transition with the following long right-twisted blade of 180° twist.
- Analogous, in the *upper section* the 180° right-twisted blade forms a R-L transition with the following 90° left-twisted blade that smoothly changes into the exit duct.

This configuration contains all necessary elements and there is no need to separately compute a velocity field around a long-left-twisted blade, since it is the mirror image of that of the right-twisted blade. Similarly, the effect of the L-L and L-R transition is completely defined by their mirror counterparts (R-R and R-L transitions, respectively).

Fig. 3B shows the surface of the finite element mesh used to compute the velocity field, containing 13,824 second-order hexagonal elements with 116,145 nodal points (403,731 degrees of freedom). At the rigid walls a no-slip boundary condition is prescribed and at both inlet and outlet, a fully developed

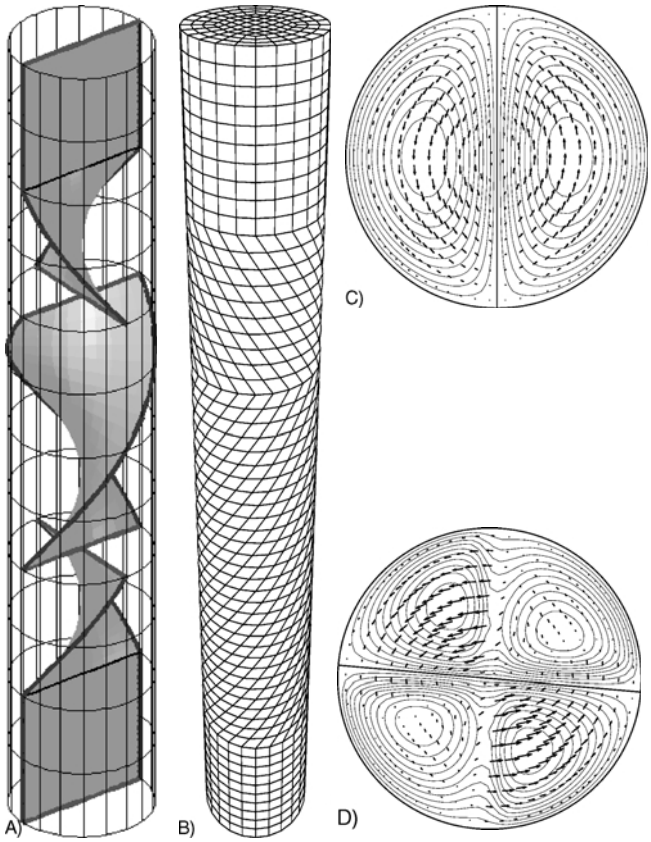

Fig. 3. Computing the velocity field patterns in the Kenics, A: the flow domain; B: the finite element grid; C: the velocities at the cross-section in the middle of the long blade; D: the same, but slightly below the R-L transition. The contours in (C) and (D) are isolines of the axial velocity u_z, the arrows show the lateral velocity components

Poiseuille profile is prescribed. The fluid is assumed to be Newtonian with a constant viscosity, unless explicitly stated otherwise. Under these conditions the axial velocity in the Stokes flow through a vertical semicircular duct $x^2 + y^2 < a^2$, $y > 0$ of the radius a can be expressed by the exact analytical formula [11]. In polar coordinates (r, θ) it reads:

$$
\begin{aligned}
u_z = {} & \frac{2\pi}{\pi^2 - 8}\langle u_z\rangle \\
& \times\left\{-\pi\frac{r^2}{a^2}\sin^2\theta + \left(\frac{r}{a} - \frac{a}{r}\right)\sin\theta - \frac{1}{4}\left(\frac{r^2}{a^2} - \frac{a^2}{r^2}\right)\sin(2\theta)\right. \\
& \times \ln\frac{r^2 + 2ar\cos\theta + a^2}{r^2 - 2ar\cos\theta + a^2} \\
& \left. + \frac{1}{2}\left[2 - \left(\frac{r^2}{a^2} - \frac{a^2}{r^2}\right)\cos(2\theta)\right]\arctan\frac{2ar\sin\theta}{a^2 - r^2}\right\}, \qquad (1)
\end{aligned}
$$

where $\langle u_z\rangle$ denotes the average axial velocity. A conjugate gradient solver, implemented in the SEPRAN finite element package [18] was used to obtain the velocity field inside the mixer. The solution was then exported from SEPRAN and customary optimized interpolation routines were used to obtain the velocityin an arbitrary point inside the fluid domain.

Two typical examples of the velocity field are given in Figs. 3C, D. In both images, the contours are isolines of the axial velocity u_z and the arrows indicate the lateral velocity components. The upper right image, Fig. 3C shows the velocities in the mixer cross-section, located in the middle of the long blade. Interesting is that the distribution of the axial velocity is very close to the Poiseuille profile for a straight semicircular duct [11]. Close to the end of the blade the picture, however, changes significantly and an example of the velocity field slightly below the R-L transition (at the distance that corresponds to 5° turn of the blade) is given in Fig. 3D. The vicinity of the next blade, with opposite twist, not only changes the axial velocity profile, that now has four maxima, but also suppresses the lateral velocity in the zones, where the fluid is approaching the surface of the next blade.

2.2 Mixing Modules

It is necessary to verify our assumption that the mixer can be represented as a sequence of modules, some describing the transition regions of blade junctions, others just sections of different lengths with undisturbed velocity fields. To find the distance from the transitions where the flow can be regarded as undisturbed, the velocity field was analyzed in more detail, close to and away from R-R and R-L transitions. A rotational transformation was applied to bring all cross-sections to the same orientation and the deviation of the velocity fields from the reference velocity field, taken in the middle of long blade, was analyzed. This deviation is defined as

$$\delta v = \sqrt{\frac{1}{N}\sum_{i=1}^{N} |\vec{u}^i - \vec{u_0}^i|^2}, \qquad (2)$$

where $\vec{u}^i$ and $\vec{u_0}^i$ are the velocities at the same location (point number i) in the disturbed and undisturbed (at the middle of long blade) velocity field, on a grid of $N = 1600$ points, distributed evenly over the cross-section. Its value, scaled with the average of the absolute value of velocity $\langle v \rangle$, is plotted in Fig. 4A versus the distance from the middle of the blade, which for convenience is transformed into the turn angle of the blade. Based on these estimations the transition zones are defined as spanning the distance corresponding to a 45° turn of the blade. (The transition zones were even increased in some tests to 60° in order to minimize errors and to verify the optimization results. These changes did not make a noticeable difference.) Far from the transition zones the velocity field will be copied (with rotational and reflectional transformations) from the reference cross-section.

As will be pointed out in subsection 2.3 the flow tubes must be traced in order to obtain the mapping matrix coefficients. The contours enclosing the flow tube are represented by polygons and are tracked using an adaptive front tracking scheme [19], until they reach the final cross-section. The residence time for various markers may differ significantly and grows unbounded for markers adjacent to the walls, which makes straightforward tracking complicated. However, since it was found that regions of back flow are not present in a Kenics mixer, and thus the axial velocity u_z is positive at any point not located on the solid surface, it is possible to follow the trajectory of particles by using the axial coordinate, rather than time, for integrating the equations of motion. Along the path line of a particle the derivatives of transversal coordinates x and y are:

$$\frac{dx}{dz} = \frac{u_x}{u_z}, \qquad \frac{dy}{dz} = \frac{u_y}{u_z}. \qquad (3)$$

These derivatives behave smoothly inside the computational domain and have well-defined limits at the boundaries. Thus, to facilitate the tracking computations, when a marker is located too close to the boundary (closer than $d = 0.0017R$, where R is the tube radius), the derivatives (3) are replaced by their values at the nearest internal point located in the same cross-section at the distance d from the wall. After these simplifications, Eq. 3 are easily integrated numerically over z using an adaptive Runge-Kutta scheme.

Fig. 4B shows the secondary flow, described by Eq. 3 in the middle of the long blade, obtained by subtracting the helical motion that would be caused by rotation together with the blade. It is clearly seen that the material is being rotated (necessarily deforming) in each of the channels. Note that the plotted vectors are not approaching zero values close to the walls, since they were re-scaled with u_z, which itself approaches zero there. This relative pattern shows that material striations, being cut by the blade, are transported in opposite directions along the blade: the behaviour clearly recognizable in the experimental results of [3].

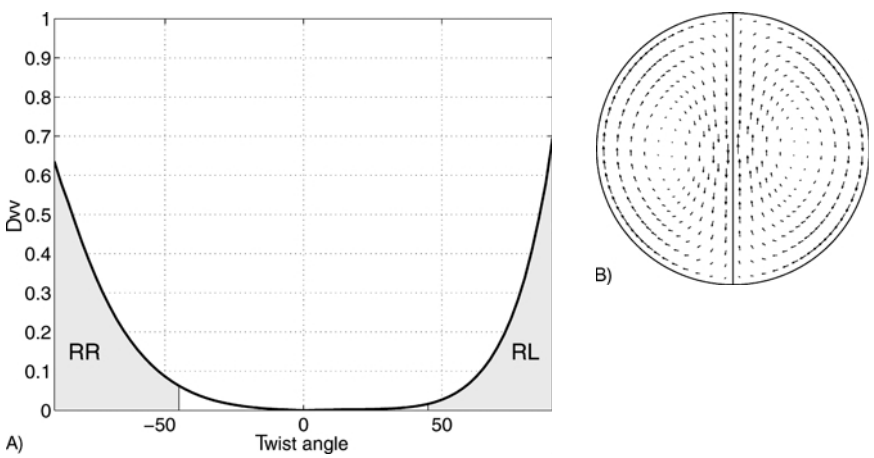

Fig. 4. Defining the modules for assembling different mixer configurations, A: finding how far the disturbances from blade transitions reach. B: revealing the secondary flow in undisturbed region. The scaled velocities (3) are shown

2.3 Mapping Matrices

The "mapping" method is proposed based on the original ideas of *Spencer* and *Wiley* [20], and the main idea is not to track each material volume in the flow domain separately, but to create a discretized mapping from a reference grid to a deformed grid. Within the mapping method a flow domain is subdivided into N non-overlapping sub-domains Ω_i with boundaries $\partial\Omega_i$, see the example in Fig. 5. The boundaries $\partial\Omega_i$ of these sub-domains are represented by polygons and tracked from $z = z_0$ to $z = z_0 + \Delta z$ using an adaptive front tracking model [19], and, as a result, deformed polygons are obtained. The area of the intersections of the deformed sub-domains with the original ones, determine the elements of the mapping (or distribution) matrix Ψ, where Ψ_{ij} equals the fraction of the deformed sub-domain $\partial\Omega_j$ at time $z = z_0 + \Delta z$ that is found in the original ($z = z_0$) sub-domain Ω_i:

$$\Psi_{ij} = \int_{\Omega_j|z=z_0+\Delta z \bigcap \Omega_j|z=z_0} d\Omega \Big/ \int_{\Omega_j|z=z_0} d\Omega \qquad (4)$$

and are computed using the polygonal descriptions of the sub-domains. For details on the validation and accuracy of the mapping method we refer to [21].

The sub-domain grid, used in determining the mapping matrices, contains 1.6×10^5 cells and has the same structure as the coarse grid, shown in Fig. 5. The fact that the grid is structured makes it computationally inexpensive to find in which cell any specified point is located and what its neighbouring cells are (which is essential for a fast computation of the mapping matrix).

Fig. 6 shows schematically the parts of mixer, described by the computed matrices (the modules). The matrices denoted as RR1 and RR2 represent the sections with 45° blade twist (see Fig. 4) of the transition zones around the R-R transition. Similarly, RL1 and RL2 matrices describe the R-L transition. Different matrices representing various amount of twist of the long R blade were computed, to be precise matrices describing $5°, 10°, 15°, \ldots, 90°$ twist were used. In Fig. 6 the block, represented by the matrix R90 (90° twist of the right-turning blade) is marked. A total blade twist of 90° is the minimum value in our optimization (entrance and exit transition zones of 45° each, without an additional module in between). Symmetry (mirroring transformation) is used to obtain the matrices for the L-L and L-R transitions and for the left-twisted long L blade.

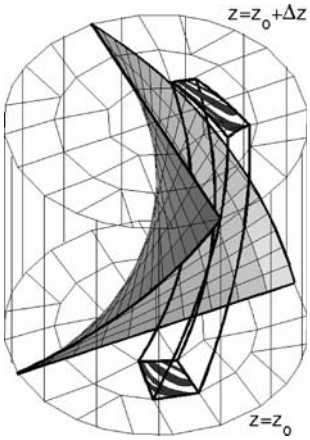

Fig. 5. Computing the mapping matrix coefficient Ψ_{ij}: the initial sub-domain Ω_j is tracked and the intersection of the deformed Ω'_j after tracking with Ω_i is determined

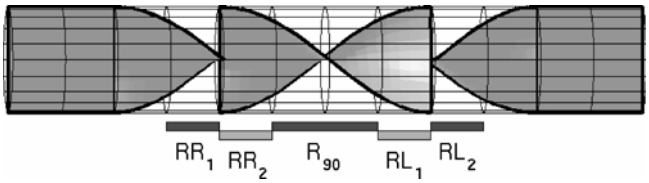

Fig. 6. Scheme if the "building blocks" of Kenics mixers

When the sparse matrix is determined, its storage is converted into a more conventional column-oriented physically ordered packing, similar to what is done in many commercial packages. Note, that the sparse storage is essential for using the mapping approach. For example the full matrix, describing a 90° twist of the long blade, would contain 2.56×10^{10} elements and would require over 200 Gb of storage memory. At the same time the flexible storage, used during the computation of the matrix, only requires 14.8 Mb, while the last, more compact storage algorithm, reduces this value even further to just 11.3 Mb. This makes a simultaneous storage in RAM possible, as well as handling of multiple matrices simultaneously, on a modern PC. Loading of a matrix from the disk file typically requires a few seconds.

While the determination of the mapping matrices required takes some effort (up to 20 hours cumulative CPU time), a single mapping operation requires only a fraction of a second of CPU time (of the order of 0.1 second on AMD Athlon^{tm}1.0 GHz). Thus, mapping makes it possible to evaluate a large number of mixer layouts and to proceed with a large number of blades, while still obtaining the material striations.

3 Macroscopic Homogenization

3.1 Intensity of Segregation

In order to be able to quantitatively compare different mixtures and, thus, to compare the performance of mixers with various layout, we use the *flux-weighed*, *slice-averaged*, *discrete intensity of segregation* defined in a cross-section, using coarse grain concentrations c_i in the cells:

$$\mathcal{I} = \frac{1}{\bar{c}(1-\bar{c})} \frac{1}{F} \sum_{i=1}^{N} (c_i - \bar{c})^2 f_i,$$

$$\text{where} \quad \bar{c} = \frac{1}{F} \sum_{i=1}^{N} c_i f_i, \quad F = \sum_{i=1}^{N} f_i, \qquad (5)$$

where f_i is the volumetric flux through the cell number i and F is the total flux through the mixer. The intensity of segregation is equal to 1 for an unmixed (only white and black cells) distribution and falls to $\mathcal{I} = 0$ for a uniform gray pattern.

Note, that this flux-weighed definition (5) of the intensity of segregation (as opposed to the area- or volume-weighed definitions used in 2D and 3D closed prototype flows in [7, 22]) is

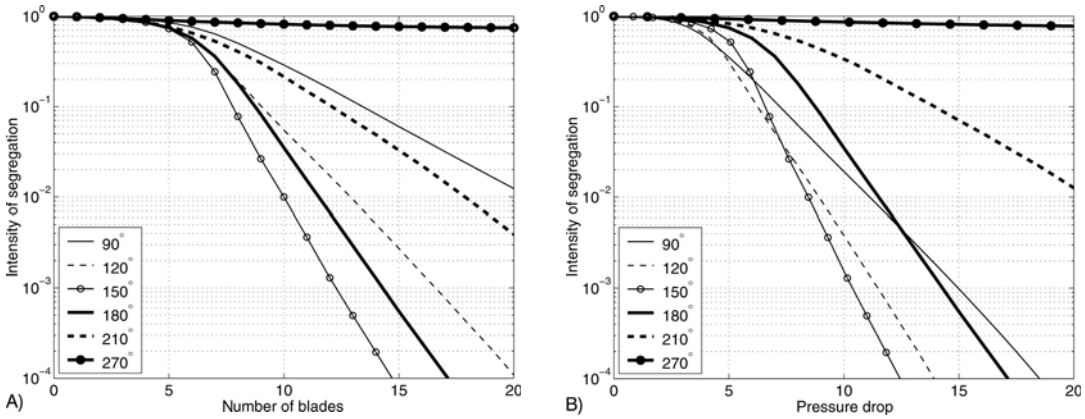

Fig. 7. Dependence of the intensity of segregation on number of blades (A) and on scaled pressure drop (B) for RL mixers with different blade twist angle

much better suited for analyzing continuous mixers, since the real influence of an unmixed spot on the value of $\mathcal{I}$ is proportional to the flux, carried through this spot. The results of using definition (5) may be somewhat different from the visual impression of the concentration distribution in slices inside the mixer, since the unmixed patches near the mixer walls, and especially in the corners between the blade and the pipe surface, are carrying very little flux, as compared to the inner parts of the channels. One should, though, remember that any decrease in the computed intensity of segregation is caused by two factors: first, the actual homogenization due to mixing and, second, numerical diffusion of the mapping method due to concentration averaging in every sub-domain after each mapping step. Thus, the absolute value of $\mathcal{I}$ is only indicative. However, comparison of the evolution (rate of decrease) of the intensity of segregation for similar mixers allows to reveal the configuration that achieves the fastest mixing. This is optimization. We will compare the results of mapping with more standard methods like Poincaŕe sections and, moreover, use the *scale of segregation*, or, alternatively, the so-called *structure radius* [15, 23] to evaluate the size of the largest unmixed regions.

Since an ideal mixture is characterized by an intensity of segregation equal to zero, the rate of its (typically exponential) decrease essentially characterizes the mixer efficiency. The dependence of $\mathcal{I}$ on the axial position, represented by the number of blades, is illustrated for an RL mixer with different blade twist angle in Fig. 7A. It clearly shows that in most of the cases exponential mixing is indeed realized, but that the slopes, the rates of mixing, vary significantly with the total blade twist angle. This plot does not actually provide information about the mixer *energy efficiency*, since mixers with a higher total blade twist (longer blades) also require more energy to operate due to larger pressure drop required. Nevertheless, the extremely low decrease rate of the intensity of segregation for e. g. the mixer with 270° twist gives a good indication that this configuration probably has "dead" zones of regular motion, separated by KAM boundaries [1]. Fluid contained in such zones does not mix with the rest of the flow.

Fig. 7B presents the same data as Fig. 7A, but now $\mathcal{I}$ is plotted versus the total pressure drop, given in relative units, scaled with the absolute value of pressure drop ΔP^* along one blade of the "standard" RL-180 mixer. Among the configurations presented in both plots of Fig. 7, the mixer with the blade twist angle equal to 150° achieves the highest mixture homogeneity at the lowest pressure drop.

A more precise evaluation was performed by investigating mixer configurations with a blade twist ranging from 90° to 360° with a step of 5°. The results are summarized in Fig. 8, where the logarithm of intensity of segregation is plotted as a function of pressure drop ΔP (measured in the same units as in Fig. 7B) and the blade twist angle θ. This three-dimensional plot exhibits a distinctive *valley*, the bottom of which, in the region of the larger pressure drops ΔP, is located around the value of blade twist angle $\theta = 140°$. The small "ripple" visible along the $\theta = 180°$ is caused by the fact that for the configurations with larger θ, every blade is modeled with the use of more then three mapping matrices (as for smaller values), causing a slight increase in the "numerical diffusion", introduced by the mapping computations (more mapping operations mean more per-cell averaging). This, however, does not alter the general trend. Sub-figures a–f of the Fig. 8 illustrate the mixture patterns, created by mixers with different θ at roughly the same pressure drop. For illustration purposes the pressure drop chosen is relatively low. The mixer with $\theta = 90°$ creates noticeable "irregularities" in large regions near the tube surface close to the blades. This effect is milder for $\theta = 120°$ and, for the optimal configuration with $\theta = 140°$, these badly mixed zones are small and packed closely to the channel corners. At this location their influence on mixer performance is minimal, since the flux through these zones is low. The mixer with the traditional value of $\theta = 180°$ performs well, achieving good distributions, but due to increased pressure drop per blade, it is less energy-efficient. Finally, it is clear that the poor mixing at higher θ values, around $\theta = 270°$ (see Fig. 8E), corresponds to systems with large regular, dead, zones. With further increase of the blade twist angle, the mixer seems to work again, but the high pressure drops required render it inefficient. From Fig. 8 it can be concluded that the preferable blade twist angle for a RL Kenics mixer, with the pitch angle considered in this paper (the same as in [3]), operated at close to zero Reynolds number, with Newtonian fluids, should be $\theta = 140°$. The more traditional value of the blade twist, $\theta = 180°$, corresponds to a sharp slope of the valley in Fig. 8 (line d) and small changes of parameters can be expected to have a strong influence on its performance, although not necessarily deteriorating it.

Fig. 9 is similar to Fig. 8 but describes the behaviour of RR mixer. The RR mixer with $\theta = 180°$ is unable to homogenize

components because it possesses rather large unmixed islands, which are also present for a wide range of blade twist values. Not all RR configurations of the Kenics mixer are suffering from large "dead" zones, see e. g. the RR-110 configuration, although its efficiency is still noticeably lower than that of the RL-140 mixer.

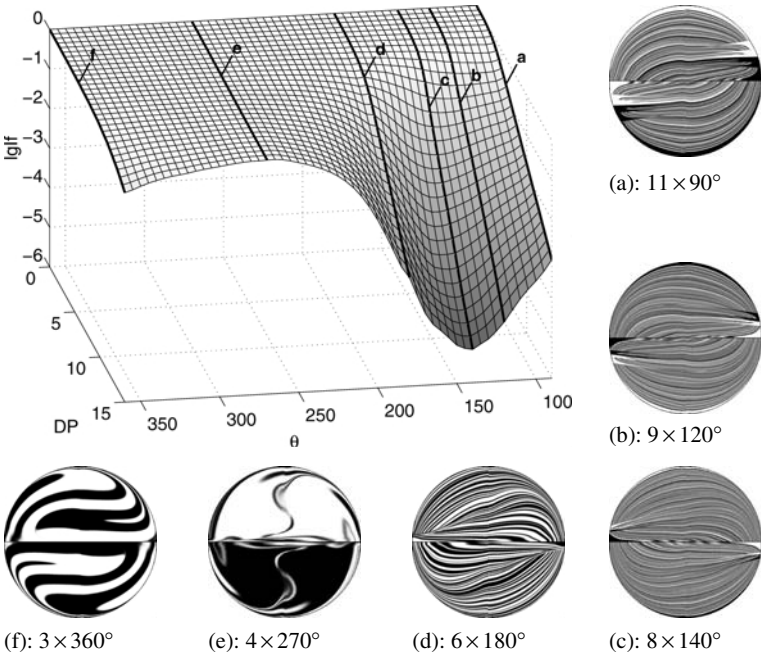

(a): 11×90° (b): 9×120° (c): 8×140° (d): 6×180° (e): 4×270° (f): 3×360°

Fig. 8. Optimization of the blade twist angle for RL mixer (Newtonian fluid): logarithm of the intensity of segregation is plotted as a function of the blade twist angle and total pressure drop

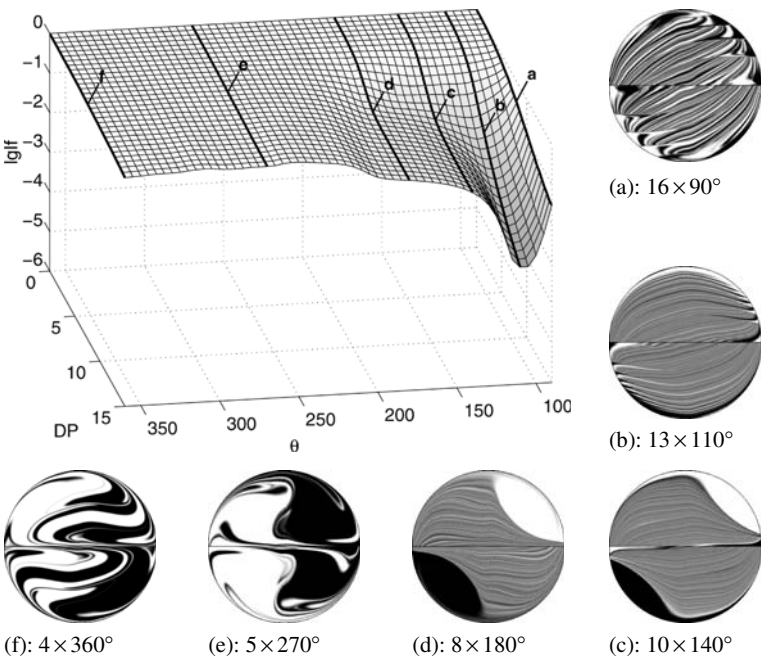

(a): 16×90° (b): 13×110° (c): 10×140° (d): 8×180° (e): 5×270° (f): 4×360°

Fig. 9. Optimization of the blade twist angle for the RR mixer (Newtonian fluid). The scale is the same as in Fig. 8, while the concentration profiles correspond to on average 30 % larger pressure drop then those shown in Fig. 8

From a mixing point of view the RR mixer is much less interesting than the RL mixer. However, some other interesting applications come to mind if we examine the RR-180 concentration patterns. This typical configuration of the Kenics mixer can be used to create rather specific structures where two polymers with different properties are mixed in the core of mixer, enclosed by two large unmixed regions each containing the pure polymer components. Examples of possible technological applications are:

(i) controlled curling of fibers, mimicking natural wool, by using two polymers with different thermal shrinkage, that are, though, closely interconnected in the middle part, and,

(ii) using a combination of conductive and non-conductive polymers to produce capacitors etc.

3.2 Influence of a Shear-rate Dependent Viscosity

The results, presented in the previous section were obtained for Stokes flows of a Newtonian fluid. It is of interest to see how the rheological properties of the fluid affect the analysis and the optimization results. In *Anderson* et al. [24] the influence of a shear-rate-dependent viscosity on mixing quality was examined in time-periodic cavity flows. For different mixing protocols the non-Newtonian behaviour could lead to both considerably better and worse mixing compared to the Newtonian case. *Fan* et al. [25] reported similar results for the journal bearing flow. Here, we study the influence of a shear-rate-dependent viscosity on the mixing performance of Kenics mixers and the viscosity η of the fluid is described by Carreau-Yasuda model with zero infinite-shear viscosity (see e. g. [26]):

$$\eta = \eta_0 \left[1 + \lambda^2 |II_{2D}|\right]^{\frac{n-1}{2}}, \qquad (6)$$

where η_0 is the viscosity at zero shear rate, $|II_{2D}|$ is the second invariant of the rate of deformation tensor and λ and $0 \leq n \leq 1$ are parameters of the model. In the examples below, the total volumetric flux through the mixer is kept the same as before, so that the average axial velocity $\langle u_z \rangle = 1$. The parameter λ is fixed at $\lambda = 10$, which ensures that we indeed enter the shear thinning region, and the power coefficient n is varied. Decreasing the power parameter n in Eq. 6 makes the axial flow profile more plug-like, see Fig. 10A. The change of the power parameter, while maintaining a constant flux, also results in a change of the pressure drop, which is illustrated in the table in Fig. 10B. Here the pressure drops corresponding to the first 45° of the blade next to the RR or RL transition (ΔP_{RR} and ΔP_{RL}, respectively) and the pressure drop $\Delta P_{90°}$ along the 90° twisted piece of long blade, are given. For comparison, the pressure drop ΔP^* at one blade of the RL-180 mixeris also presented. The changes in pressure drop are relevant, since a constant total pressure drop is chosen as a criterion in determining the optimal blade twist.

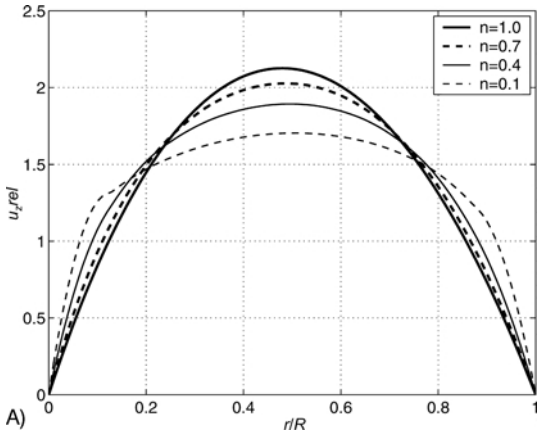

n	ΔP_{RR}	$\Delta P_{90°}$	ΔP_{RL}	ΔP^*
1.0	0.2488	0.4621	0.2690	1.0000
0.7	0.1698	0.3216	0.1825	0.6865
0.4	0.1150	0.2209	0.1227	0.4663
0.1	0.0759	0.1461	0.0803	0.3068

B)

Fig. 10. The influence of the shear thinning fluid behaviour on the performance of the Kenics mixer, (A) axial velocity along the radius, perpendicular to the blade in the middle cross section of long blade section; (B) pressure drop in the various sections of the mixer, scaled on the pressure drop on a single blade of RL-180 mixer with Newtonian (n =1.0) fluid

Mapping computations, revealing the dependence of the intensity of segregation on pressure drop and blade twist angle of the RL mixer, were performed for four different values of the power parameter n = 1.0, 0.7, 0.4 and 0.1. The evolution of the intensity of segregation for some RL mixers is shown in Fig. 11 versus the number of blades and versus pressure drop Δp respectively. Note that for the large values of the twist angle the strong shear thinning behaviour can improve the mixer performance, while for small twist angles it deteriorates the achieved mixture quality. The results of similar computations for different blade twist angles are summarized in the next figure. The left plot in Fig. 12 shows the intensity of segregation versus the blade twist angle θ, achieved at cost of apressure drop ΔP equivalent to 12 blades of the RL-180 mixer for the particular fluid, for four values of n. While the fluids with smaller n require lower pressure drops, the effect of shear thinning on the optimal blade twist is rather moderate. According to Fig. 12, shear thinning slightly shifts the optimum towards a larger blade twist and, in general, somewhat reduces the efficiency of the mixer. As an illustration, the concentration patterns after 6 blades of the RL-140 mixer for the Newtonian fluid (n = 1) and shear thinning fluid with n = 0.1 are also shown in Fig. 12. These cross-sections look remarkably similar, except for larger striation thicknesses near the walls for the shear thinning fluid. Their influence on the mixture quality (intensity of segregation) is stronger than it seems based on just a comparison of the two slices, since the shear thinning flow with its more plug-like profile (see Fig. 10A), carries the thicker near-wall striations with a larger relative flux. [23] performed the experiments with different shear-thinning fluids,

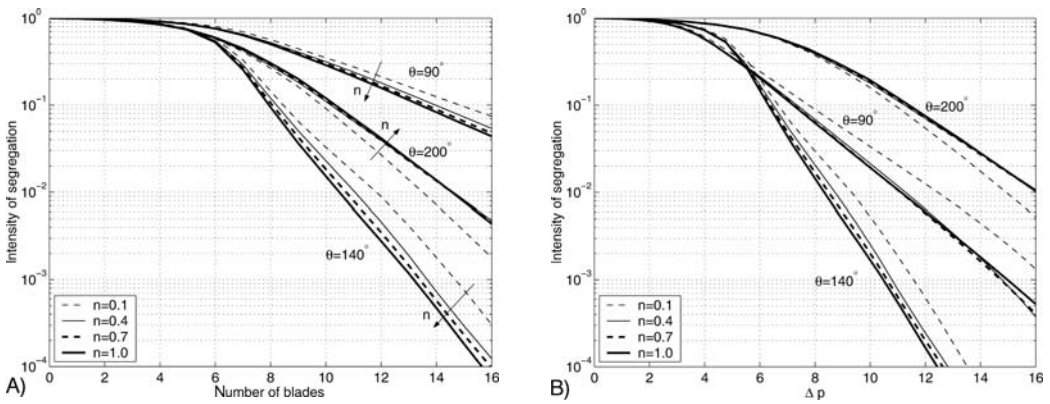

Fig. 11. Dependence of the intensity of segregation on number of blades (A) and on scaled pressure drop (B) for some RL mixers and its dependence on shear thinning behaviour

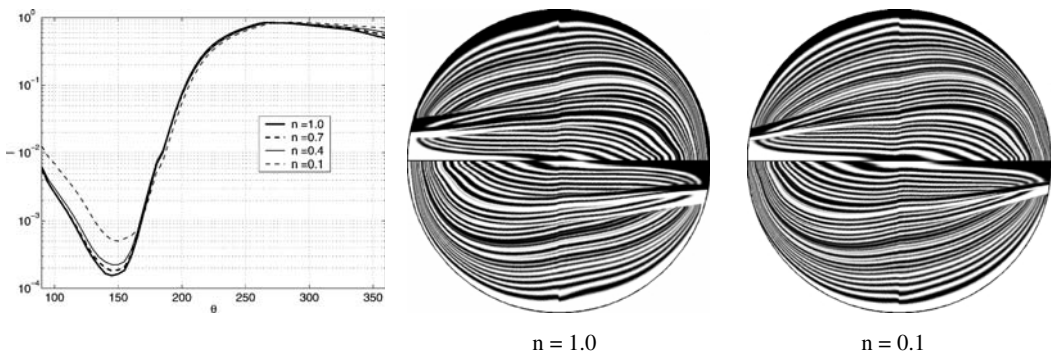

Fig. 12. Dependence of the RL mixer efficiency on the blade twist angle θ for different shear thinning parameter n. Intensity of segregation is plotted for the pressure drop equal to that of 12 blades of RL-180 mixer for the corresponding liquid. Concentration profiles are shown for n = 1.0 and n =0.1 after 6 blades

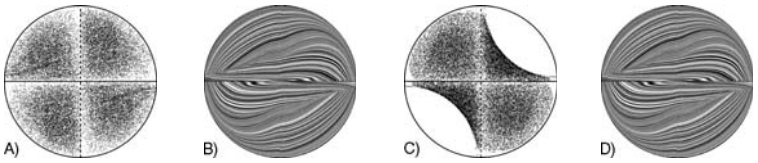

Fig. 13. Poincaré maps (A, C) compared with the concentration patterns for corresponding flows (B, D). Concentration patterns are shown after eight blades in both cases

and the influence of shear-thinning behaviour on the mixture patterns (structure radii were compared) also turned to be rather minor.

3.3 Alternative Methods and Mixture Quality Measures

One of the classical dynamical tools to analyse chaotic mixing is the Poincaŕe map. In Fig. 13 the concentration patterns after eight blades of RL and RR mixers, with blade twist $\theta = 180°$, are compared with the corresponding Poincaŕe maps. The regular islands (white regions) revealed by the Poincaŕe map (Fig. 13C) for the RR-180 configuration match the unmixed regions revealed on the concentration slice (Fig. 13D) obtained using the mapping method for the same flow. The Poincaŕe map for RL-180 configuration indicates that this system is globally chaotic, which is in complete agreement with the mapping results. The lower density of markers in Poincaŕe maps near the trailing and leading edge of the blades (cross-like patterns) is caused by significantly lower axial velocities there.

Until now we only applied the intensity of segregation $\mathcal{I}$ as a measure of the mixing quality. This mixing measure is well suited to compare the rate of mixing processes and the final mixtures, and it is the obvious tool for optimization strategies, as clearly demonstrated above. However, $\mathcal{I}$ does not provide a quantitative measure of the size of unmixed regions in the mixture. In particular if we are interested in scale-up of mixing devices this becomes important, since, for example, in geometrical up-scaling of the Kenics mixer, $\mathcal{I}$ will remain the same, while the structure radius will be proportional to the mixer diameter. A mixing measure which is related to the structure of the mixture and which provides a quantitative measure of the size of unmixed regions is the *scale of segregation*. This mixing measure is statistical in nature and was originally suggested by [27]. The definition of the scale of segregation is based on the so-called correlation coefficient (normalized correlation function), defined over the field of concentration $c(\vec{x})$ as [28]:

$$\rho(\vec{r}) = \frac{\langle [c(\vec{x}) - \bar{c}]\ [c(\vec{x}+\vec{r}) - \bar{c}] \rangle}{\langle [c(\vec{x}) - \bar{c}]\ [c(\vec{x}) - \bar{c}] \rangle}, \tag{7}$$

where $\bar{c}$ is the average concentration and the angular brackets denote an averaging over the whole flow domain, i. e. over all values of $\vec{x}$. The scale of segregation, $\mathcal{S}$, is normally used for so-called *clumpy mixtures* [28], where the correlogram is non-negative and equals zero for $|\vec{r}|$ greater than some value. $\mathcal{S}$ is defined as the volume under the correlogram:

$$\mathcal{S}(\vec{x}) = \int \rho(\vec{r})\ \mathrm{d}\mathcal{S}. \tag{8}$$

A practical way to compute the correlation coefficient, described by *Tucker* [28], involves the computation of the power spectrum of the concentration distribution using fast Fourier transformations (FFT). In order to do so for the mixture patterns obtained in the Kenics mixer, the concentration slices were padded by the area of anideal mixture $c = \bar{c}$ to obtain a square domain and re-discretized using a 1024×1024 uniform rectangular grid. Next, the two-dimensional FFT can be applied.

The correlogram obtained after four blades of RL-180 mixer (Fig. 14A), when the lamellar structure is well developed, shows a narrow central maximum and, typical for layered mixtures, an oscillating behaviour of $\rho(r)$. The plot is arranged in such a way that the point $r = 0$ corresponds to the center of the image. Fig. 14B shows the correlogram of the mixture after eight blades of the RR-180 mixer. The presence of the unmixed islands (and roughly their orientation) is indicated by the wide central maximum, while other details of the mixture are already lost.

The mixture patterns created by static mixers typically exhibit a lamellar (that is *ordered* – not a *clumpy*) structure and the correlation coefficient is oscillating taking both positive and negative values. We can extend the definition (8) of the scale of segregation $\mathcal{S}$ for the case under study by computing only the integral of the correlation coefficient $\rho(\vec{r})$ within the central maximum. We used the isoline $\rho(\vec{r}) = 0.1$ as the boundary of this maximum to avoid numerical problems (influence of small

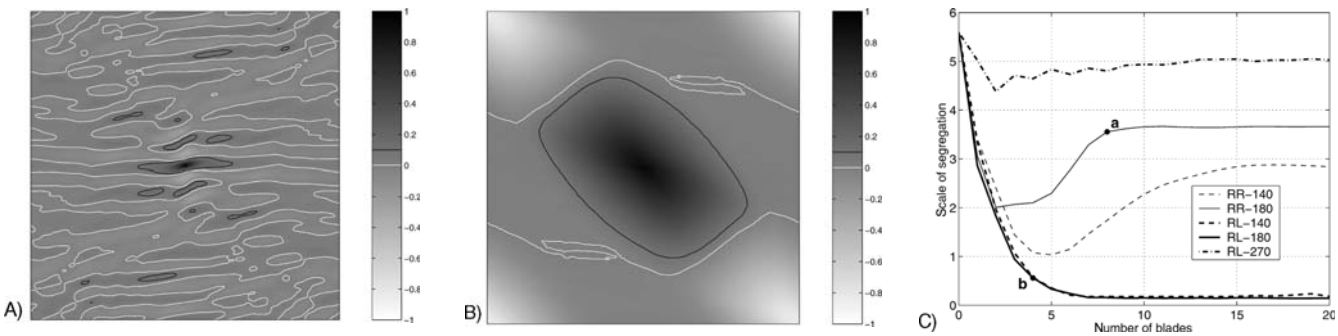

Fig. 14. The correlograms for the mixtures obtained after four blades of RL-180 mixer, (A) and after eight blades of RR-180 mixer (B) and the dependence of the scale of segregation on the number of blades for few mixer layouts (C). The white contour on correlograms correspond to $\rho > 0.1$. The scale of segregation was computed as an integral of the correlation coefficient within such a zone in the center

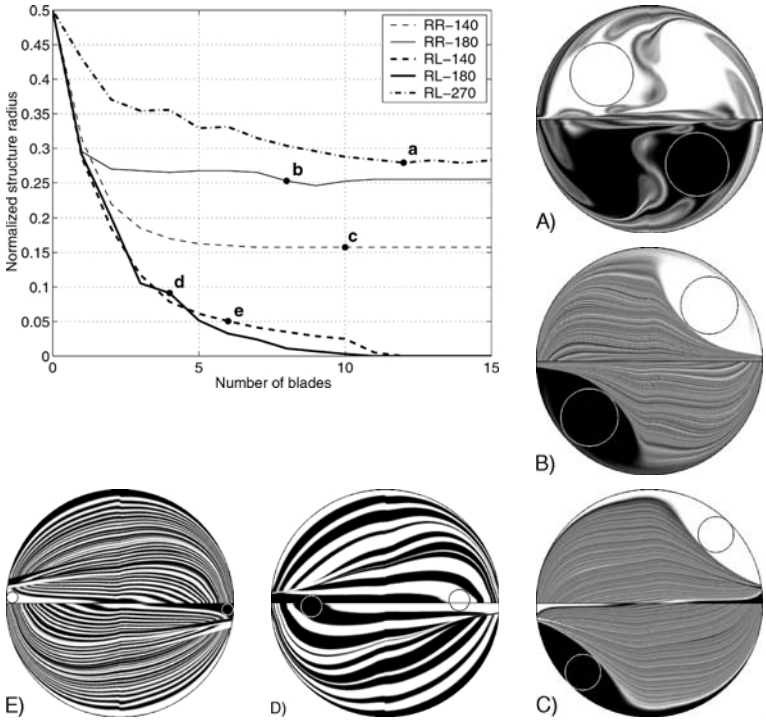

Fig. 15. Dependence of the structure radius (scaled with the mixer diameter) on the number of blades of various Kenics configurations and examples of the structure radius detection (A to E)

errors). Fig. 14C shows the dependence of the computed scale of segregation on the number of blades for a few mixer layouts. It clearly indicates the presence of islands in two mixers with blades twisted in the same direction (RR-140 and RR-180) and in the RL-270 mixer with a large blade twist. The asymptotic level of the scale of segregation also gives an estimation of the size of unmixed zones for the particular mixer geometry. However, this mixture parameter seems not so useful to rank the globally chaotic flows according to their efficiency.

Another mixing measure for the scale of the unmixed regions that is used is the *structure radius*, defined as the maximum radius of a circle that can be drawn in a concentration slice that contains only one, unmixed, fluid component [15, 23]. Fig. 15 gives some examples of the structure radius and shows its evolution with the number of blades for a few mixer configurations. The markers indicate the situations for which the concentration slices (a – e) are shown. The evolution of the structure radius provides some essential information, quickly showing the flows with regular islands: for these flows the structure radius reaches some non-zero constant value. This mixture quality parameter is also less suitable for comparing the efficiency of different mixer configurations, since it only shows the size of the unmixed patch but not the flux, carried by it. For example, it overestimates the importance of unmixed "corners" in Fig. 15E obtained for the RL-140 mixer. These unmixed patches carry a much smaller flux than the patches of similar size at any other location will do. Another obvious disadvantage of this criterium is its computational cost: to compute the structure radius requires significantly more CPU time than a single loop over all sub-domains, as it is the case for the intensity of segregation. Moreover, the analysis of the less mixed patterns, with large unmixed patches, requires a large number of operations, roughly (since the subdomain grid is not uniform) proportional to the square of the structure radius. Nevertheless the structure radius provides a useful, and physically meaningful, tool that can be used during scale-up evaluations of different mixers. This is illustrated in Fig. 16, which shows the dependence of the structure radius on the mixer length for two different mixers: the reference RL-180 configuration and its two times larger copy. From these results one can determine, for example, that, in order to achieve the same value 0.1 of the structure radius, an approximately three times larger length (1.5 times more blades) of the larger mixer would be required.

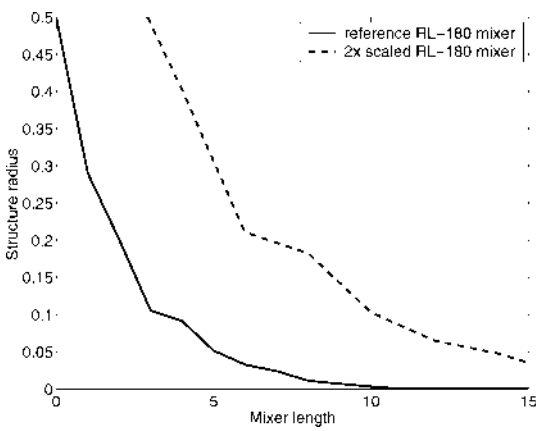

Fig. 16. Scale-up evaluation of the RL-180 mixer: dependence of the structure radius (scaled with the diameter of the reference mixer) on the mixer length. The mixer length is scaled with the length of one blade of the reference mixer

4 Near-wall Material Exchange

4.1 Removing Material from the Pipe Surface

A problem that also could occur in Kenics mixer is the formation of a degraded material layer on the pipe surface due to high residence times. Thus, it is of interest to examine how the material initially located near the pipe surface is being advected (whether it leaves the near-wall region and in what time). The stagnation and degradation at the blades is less prominent: these surfaces are *interrupted* at the trailing edges.

To evaluate the "wall cleaning" performance of Kenics mixers, a special initial pattern was used: the marked fluid initially occupies a ring adjacent to the walls (20 cells wide in 400×400 mapping grid). The initial concentration pattern is shown in Fig. 17A. Fig. 17B, C demonstrate the effect of one blade of the RL mixers with 90° and 180° blade twist, respectively. Basically, in the range explored a larger blade twist increases the wall clearing effect of a single blade.

The distribution of the material, originating from the near-wall region in the RL-140 mixer is shown after different num-

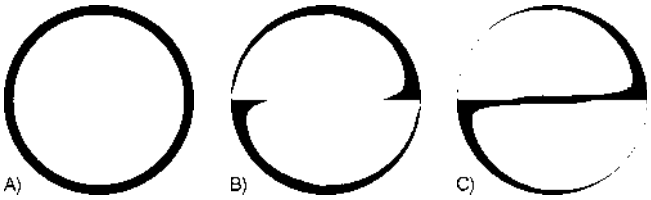

Fig. 17. The clearing of near-wall region by one blade of RL-mixer, (A) initial pattern; (B) RL-90 mixer; (C) "standard" RL-180 mixer

ber of blades in Fig. 18. It is clear that some "old" material is still on the pipe surface after six blades, and the largest non-cleared areas are near the corners.

The wall-cleaning effect of just two blades is shown in Fig. 19 for different blade twist angles from 90° to 210°. Again, we see more efficient cleaning and smaller "corner effects" in

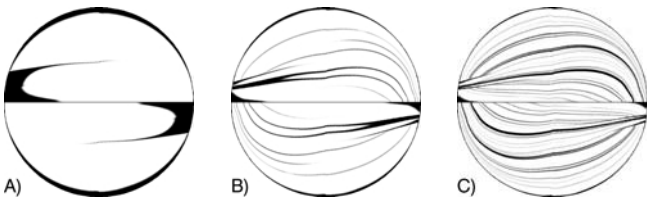

Fig. 18. The clearing of near-wall region by the RL-140 mixer, (A) two blades; (B) four blades; (C) six blades

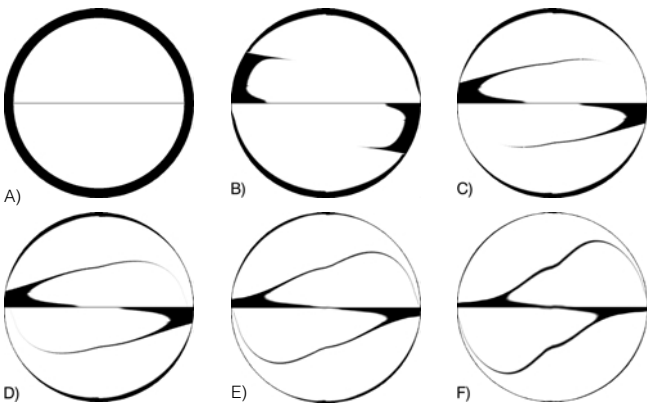

Fig. 19. The clearing of near-wall region by two blades of RL mixers, (A) initial pattern; (B) θ = 90°; (C) θ = 120°; (D) θ = 150°; (E) θ = 180°; (F) θ = 210°

case of large blade twist angles. For mixers with a large blade twist angle the exchange between the near-wall layer and the bulk of the flow is improved. The estimations can also be performed regarding the *flux* of the marked material still in the wall zone instead of the relative *area*. The area, however, may be rather relevant, since the degraded material may solidify on the wall surface (in that case it is the layer thickness that matters).

The results presented above may indicate that the mixers, achieving fast homogenization (like RL-140 layout considered earlier) may suffer from material degradation more than mixers with larger blade twist. A possible solution could be to combine short and long blades in the mixer layout, for example inserting after certain number of short blades a couple of longer ones in order to improve clearing of the pipe wall. The mapping method allows to explore different mixing layouts where the twist angles may be adjusted independently. Fig. 20 shows two examples. The first combines long 180° blades with shorter 120° blades in an alternating pattern 180°/120°/180°/120°. Although the wall cleaning performance of this layout is better then that of RL-140 mixer (see Fig. 20B), the homogenization efficiency is strongly deteriorated: the intensity of segregation decreases slower then in standard RL-180 case, as it is shown in Fig. 20A. From a number of tests performed it follows that similar configurations that have a two-blade RL repeating sequence with unequal blade twist angle generally do not mix fast. However, more complex layouts like shown in Fig. 20 RL-180/120/120/180 (the same blades in different order) do offer a compromise between, for example, good homogenization efficiency of RL-140 layout and wall cleaning features of simple RL configurations with longer blades. Depending on the degree of emphasis laid upon the homogenization efficiency and wall cleaning, various Kenics layouts may be selected.

5 Residence Time Distribution

Since material degradation due to excessive residence times or stagnation effects is an important issue in static mixers, it is also of interest to analyse the residence time distribution patterns. To include the residence time into the mapping simulations, the increment of the residence time caused by different mixing modules was computed. The interval of time required for the material originating for each donor cell of the mapping

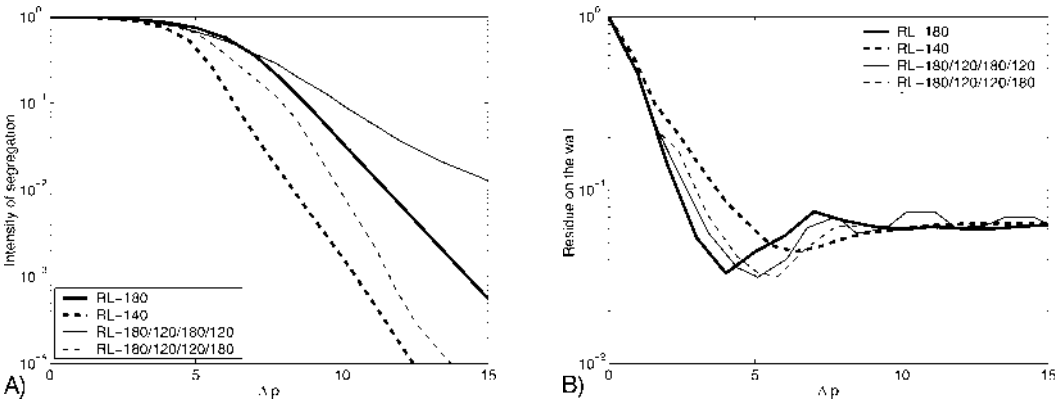

Fig. 20. The dependence of the intensity of segregation (A) and residue on the wall (B) on the pressure drop for some Kenics configurations. See text for further explanations

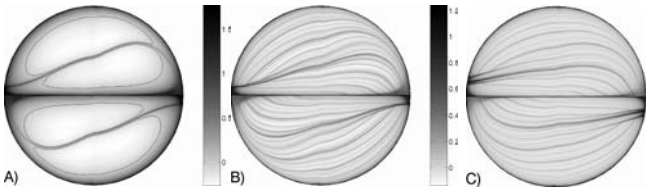

Fig. 21. The relative residence time $log_{10}(t/t^*)$ after 2 blades (A) and 14 blades (B) respectively of RL-180 mixer and after 18 blades of RL-140 (C). See text for further explanations

grid to reach the destination cross-section was computed. This time was estimated by tracking a single marker, placed initially in the centroid of the donor mapping cell. Thus, we imply that this time characterizes the whole cell. Note, that the residence time not always can be averaged over the fluid volume. In particular, the residence time of the material near the rigid wall is unbounded due to non-slip boundary conditions. As a result, the mapping technique that uses volume-averaged coarse grain values may underestimate the high values of residence time, caused by stagnation on the rigid walls. It may, nevertheless, produce useful estimations, locating "dangerous" zones. The residence time is properly incremented on every step and mapped similarly to the "wall-path", considered in section 4.

Fig. 21A illustrates the residence time distribution after two blades of the "standard" RL-140 mixer. The decimal logarithm of the relative residence time t/t^* is shown. The scaling factor is the "characteristic time" $t^* = \Delta z/\langle v_z \rangle$ during which the particle that moves with average axial velocity $\langle v_z \rangle$ would travel the length Δz of the mixer being analysed. The black contours in Fig. 21A separate the areas where the relative residence time is larger and smaller then its average value (one – according to definition). As expected, high residence times are observed near the walls, especially in the corner regions. The additional curved strip of material with high residence time, which is visible in both channels, is the trail of the previous blade.

Fig. 21B, C show the distribution of the relative residence time after 14 blades of RL-180 and after 18 blades of RL-140 mixers, respectively. These mixer layouts with the given number of blades have equal total length and, consequently, equal characteristic times. Both plots use exactly the same gray scale-map. The maximum residence times observed in the mixer with the smaller blade twist are somewhat larger then in the standard configuration. In both cases old material is concentrated near the corners of the channels. For the RL-140 mixer, however, the zones with old material are reaching further away from the blade. These results are in the qualitative agreement with the estimates obtained in section 4. Since the material with high residence times is found in the corner regions, where the velocities are low, its contribution to the total flux is rather low. If the cumulative flux of the material with a residence time lower then certain threshold is plotted as a function of this (threshold) residence time, see Fig. 22, it turns that the RL-140 mixer exhibits an even more step-like profile, as compared to the standard RL-180 configuration.

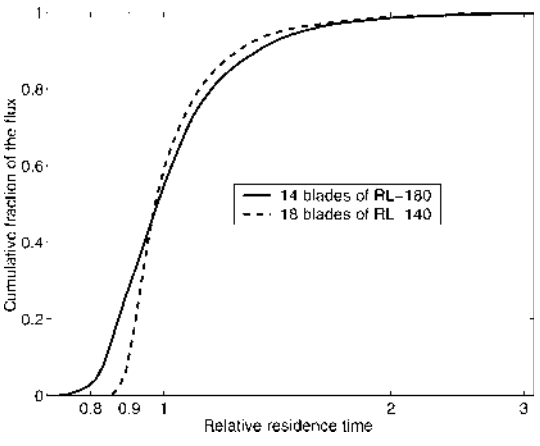

Fig. 22. The cumulative fraction of the flux of material with relative residence time below certain threshold is plotted as a function of the threshold value. These plots correspond to the residence time distributions shown in Fig. 21B, C

6 Discussion and Conclusions

The flow in the Kenics static mixer was studied and the dependence of the mixing efficiency on the most relevant geometrical parameter – the blade twist angle – was investigated. The pitch of the blades was kept constant (as in [3]) and the mixer configurations with alternating and with the same direction of blade twist were considered. The velocity field was computed using a finite element method. To enable efficient modeling of various mixer configurations, the evolution of concentration patterns was simulated using the mapping method.

Hobbs and *Muzzio* [9] studied the performance of the RL Kenics mixer for different blade twists but, since they had to recompute the velocity field every time, only a limited number of θ values could be considered ($\theta = 30°$ step $30°$ until $210°$). Using the stretching efficiency as acriterion, they concluded that a $120°$ blade twist results in the most energy efficient mixer with respect to the pressure drop required. In the current work the possibility to quickly analyze a wide range of twist angles with smaller increments ($\Delta\theta = 5°$) yielded a distinct optimal twist angle equal to $\theta = 140°$. The criterion used to find this optimum (the *volume-flux weighed, slice-averaged, discrete intensity of segregation*) seems preferable (and of more direct nature) above the one used by [9]. Moreover, the *mapping method* reveals the distinct material striations at more advanced mixing stages then it is typically achievable with marker tracking [3, 8, 9].

Shear thinning behaviour of the fluid viscosity has only a surprisingly small effect on the concentration patterns, produced by the Kenics mixer, confirming the partial results of [3]. It causes a slight increase of the optimal angle and results in a somewhat lower efficiency of the mixer. The visible effect is the increasing thickness of the near-wall material striations. In general, it appears that we can expect shear thinning to have a rather moderate effect on mixing behaviour in static mixers (pressure-driven flows). In drag-driven time-periodic cavity flows [24] a more significant effect of shear thinning on flow performance was observed.

The Kenics mixer with all blades twisted in the same direction (RR) is known to be not efficient, leaving large unmixed streaks [9]. However, it was found that in a certain range of twist angles it can also achieve global mixing, although the mixing efficiency is still noticeably lower then for the mixer

with an alternating direction of the blade twist. The computed optimal twist angle for the RR mixer was close to $\theta = 110°$. The remarkable concentration patterns, created by the RR Kenics mixer in the middle range of twist angles, with two well-defined unmixed islands separated by exponentially mixed striations in between (Fig. 9C, D) could have some interesting technological applications, other than creating a perfect mixture. The size of the unmixed regions is easily controlled by the blade twist angle.

The scale of segregation can be used to determine the size and shape of the largest unmixed regions. Its asymptotic level provides an estimation of the size of the unmixed zones for the particular mixer geometry, while the shape of the central maximum on the correlogram indicates their orientation. An alternative mixing measure that is used in literature is the *structure radius*, which has a simple geometrical meaning and is more "intuitive". It demonstrates the same trends as found before with the use of the intensity of segregation, but it requires more extensive computations for its evaluation. From these analyses of a rather traditional mixer, as the Kenics static mixer with its rather simple geometry, it can be concluded that the mapping method, combined with proper mixing quality measures, provides a powerful design tool in optimizing mixers for their performance.

References

1 *Ottino, J. M.:* The kinematics of mixing: stretching, chaos and transport. Cambridge texts in applied mathematics. Cambridge University Press (1989)
2 *Fox, R. F.:* Chaos 8, p. 462 (1998)
3 *Avalosse, Th., Crochet, M. J.:* AIChE J. 43, p. 588 (1997)
4 *Franjione, J. G., Leong, C.-W., Ottino, J. M.:* Phys. Fluids. A, 1, p. 1772 (1989)
5 *Liu, M., Peskin, R. L., Muzzio, F. J., Leong, C. W.:* AIChE J. 40, p. 1273 (1994)
6 *Anderson, P. D., Galaktionov, O. S., Peters, G. W. M., v. d. Vosse, F. N., Meijer, H. E. H.:* J. Fluid Mech. 386, p. 149 (1999)
7 *Galaktionov, O. S., Anderson, P. D., Kruijt, P. G. M., Peters, G. W. M., Meijer, H. E. H.:* Comput. Fluids 30, p. 271 (2001)
8 *Hobbs, D. M., Muzzio, F. J.:* Phys. Fluids 10, p. 1942 (1998)
9 *Hobbs, D. M., Muzzio, F. J.:* Chem. Eng. Sci. 53, p. 3199 (1998)
10 *Khakhar, D. V., Franjione, J. G., Ottino, J. M.:* Chem. Eng. Sci. 42, p. 2909 (1987)
11 *Meleshko, V. V., Galaktionov, O. S., Peters, G. W. M., Meijer, H. E. H.:* Eur. J. Mech./Part B – Fluids 18, p. 783 (1999)
12 *Hobbs, D. M., Muzzio, F. J.:* Chem. Eng. J. 67, p. 153 (1997)
13 *Hobbs, D. M., Swanson, P. D., Muzzio, F. J.:* Chem. Eng. Sci. 53, p. 1565 (1998)
14 *Hobbs, D. M., Muzzio, F. J.:* Chem. Eng. J. 70, p. 1942 (1998)
15 *Byrde, O., Sawley, M. L.:* Comput. Fluids 28, p. 1 (1999)
16 *Fourcade, E., Wadley, R., Hoefsloot, H. C. J., Green, A., Iedema, P. D.:* CFD calculation of laminar striation thinning in static mixer reactors. Chem. Eng. Sci. 56, p. 6729 (2001)
17 *Joshi, P., Nigam, K. D. P., Nauman, E. B.:* Chem. Eng. J. 59, p. 265 (1995)
18 *Segal, A.:* SEPRAN, user manual, standard problems and programming guide. Ingenieursbureau SEPRA, Leidschendam (1984)
19 *Galaktionov, O. S., Anderson, P. D., Peters, G. W. M., v. d. Vosse, F. N.:* Int. J. Numer. Meth. Fluids 32, p. 201 (2000)
20 *Spencer, R. S., Wiley, R. H.:* J. Colloid Sci. 6, p. 133 (1951)
21 *Kruijt, P. G. M., Galaktionov, O. S., Anderson, P. D., Peters, G. W. M., Meijer, H. E. H.:* Mapping method for mixing optimization, in: Heino Thiele (Ed.), VDI-K Jahrestagung, Proceeding, p. 3. VDI Verlag, Düsseldorf (2000)
22 *Kruijt, P. G. M., Galaktionov, O. S., Anderson, P. D., Peters, G. W. M., Meijer, H. E. H.:* AIChE J. 47, p. 1005 (2001)
23 *Liu, S.:* Master's thesis, McMaster University, Department of Chemical Engineering, Hamilton, Ontario (2000)
24 *Anderson, P. D., Galaktionov, O. S., Peters, G. W. M., v. d. Vosse, F. N., Meijer, H.E.H.:* J. Non-Newtonian Fluid Mech. 93, p. 265 (2000)
25 *Fan, Y., Tanner, R., Phan-thien, N.:* J. Fluid Mech. 412, p. 197 (2000)
26 *Macosko, C. W.:* Rheology: Principles, Measurements and Applications. VCH Publishers, Weinheim (1994)
27 *Danckwerts, P. V.:* Appl. Sci. Res. A 3, p. 279 (1953)
28 *Tucker III, C. L.:* Principles of Mixing Measurements, in: Mixing in Polymer Processing. Rauwendaal, C., Marcel Dekker, New York (1991)

Date received: February 3, 2003
Date accepted: February 8, 2003